Pulsed spatial switching at the interface separating Kerr-like instantaneous and relaxing dielectric media

H. Adachihara and J. V. Moloney
Department of Physics, Heriot-Watt University, Riccarton, Edinburgh EH14 4AS, Scotland

J. N. Polky
Photonic Lab, High Technology Center, Boeing Electronics, P.O. Box 24969, MS 7J-27, Seattle, Washington 98124-6269
(Received 17 October 1989)

Propagation of optical pulses, both Gaussian and square in time, at an oblique angle to the interface separating two nonlinear self-focusing media, is studied numerically. The role of a finite-medium response in determining the reflection and transmission asymptotics of the pulse is established, and it is confirmed that, in the limit of a negligible Debye relaxation time, the equivalent particle theory for cw incident beams applies. Examples of spatially distributed multiplexing and demultiplexing of optical pulse trains illustrate the usefulness of the equivalent-particle picture in designing novel optical switching architectures.

I. INTRODUCTION

The propagation of a self-trapped monochromatic cw light beam at an oblique angle of incidence to one or more interfaces separating self-focusing nonlinear media has been studied by Aceves *et al.*[1] This work established that the full beam propagation problem could be reduced to the study of the motion of an equivalent particle in an equivalent potential in certain well-defined physical limits. Contact was made in this study with earlier numerical simulations of Gaussian beam incidence at the interface separating a linear and nonlinear dielectric,[2] and it was established that many of the numerical observations of that work could be qualitatively understood in the context of the theory in Ref. 1. The main interest in light-beam reflection at single or multiple nonlinear interfaces stems from its potential application in all-optical switching and computing.[3] Moreover, as the work in Ref. 1 showed, the underlying self-trapped light channel can be treated as a perturbed spatial soliton of a modified nonlinear Schrödinger equation, whose robustness to perturbations ensures that the soliton shape remains intact, with the slow evolution of its parameters describing the reflection and transmission asymptotics of the incident self-trapped light beam. In this latter theory, the stationary TE nonlinear surface waves (NSW), computed earlier by many authors,[4] are simply stable or unstable equilibria of the equivalent potential. The role of diffusion of the material excitation on beam reflection, transmission, and trapping at a single interface separating a linear and nonlinear self-focusing medium,[5,6] and two nonlinear self-focusing media[7] has been simulated recently. Realistic all-optical switching effects will require the manipulation of short intense light pulses which may be Gaussian or square in time. The latter pulses may be produced experimentally through techniques[8] which are rapidly becoming standard. We envisage a scenario whereby two or more uniform slab nonlinear materials, with linear and nonlinear coefficients which are close in magnitude, are placed butt end to form one or more interfaces. The slab confinement in the extra dimension (y dimension, say) is necessary to prevent filamentation[9] and guarantee stable transverse soliton shapes in the unconfined x dimension. Therefore, in this paper our computations will be confined to the single transverse x dimension. Group velocity dispersion in the propagation direction will be ignored as we envisage that most applications to nonlinear optical switches will involve short propagation lengths. This configuration avoids the constraints of inflexible fabricated waveguiding structures with the transverse spatial soliton acting as a self-guided light channel. The interface serves to change the soliton parameters slowly to achieve a power controlled reconfigurable switch or spatial scanner. The present paper is concerned with solving the full time-dependent pulse reflection and transmission problem at a single interface separating two self-focusing nonlinear media. We allow, in addition, for finite material response times in each dielectric medium. One of our main objectives is to establish under what conditions the equivalent particle picture, applicable to cw beams, remains valid for pulsed operation. We find that this latter picture remains a powerful predictive tool in the limit of infinitely fast material response and still provides a good qualitative description of the pulse trajectories in the finite response limit.

The plan of the paper is as follows. The background theory is summarized in Sec. II and contact is made with the earlier soliton perturbation theory based "equivalent particle theory for cw beams" in Ref. 1. Section III presents results on optical pulse transmission, reflection, and breakup at a single nonlinear interface when the material response is instantaneous. These numerical observations are seen to be predictable by adapting the theory in Ref. 1 to the pulse problem as shown in Sec. IV. The effect of finite material response times on the reflection and transmission asymptotics of incident square and

Gaussian pulses is dealt with in Sec. V. Section VI is devoted to illustrating a novel multiplexing and/or demultiplexing application, which is again motivated by the equivalent particle picture. Our conclusions are presented in Sec. VII. Appendix A contains a short derivation of the equations and Appendix B presents details of the computational scheme used to solve these equations.

II. BACKGROUND THEORY

The numerical simulations are carried out on a nonlinear partial differential equation of the generalized nonlinear Schrödinger (NLS) type coupled to a Debye equation which accounts for a finite relaxation time of the medium. The theoretical model is directly applicable to multilayered media whose refractive indices are given by $n=n_i+\Delta n_i$ for $i=0,1,2,\ldots$. Figure 1 shows a schematic of the multiple slab geometry where we assume that the self-trapped light channel or optical pulse is incident at an angle close to the angle for total internal reflection. Because we are assuming that the refractive index increment and/or decrement from slab to slab is very small, this latter angle is very close to 90°, meaning that the self-trapped light channel is propagating essentially in the z direction. It is more appropriate therefore to discuss our results in terms of the complement of this angle.

In the paraxial approximation, the propagation of the self-focused channel is governed by the following equations:

$$2ik_0\beta\left[\frac{\partial F}{\partial z}+\frac{n_i}{\beta v_i}\frac{\partial F}{\partial t}\right]+\frac{\partial^2 F}{\partial x^2}-k_0^2[\beta^2-(n_i^2+\delta)]F=0\ ,$$
$$\tau_D\frac{\partial\delta}{\partial t}=-\delta+\alpha_i|F|^2\ , \tag{1}$$

where k_0 is the wave number of the field in the vacuum, β the effective index, v_i the group velocity of the field in medium i, τ_D the Debye relaxation time of the medium, and α_i the nonlinear coefficient of the ith medium. Both the linear refractive indices and nonlinear coefficients are assumed to change discontinuously across each interface. For simplicity, we assume a uniform relaxation time across all layers, although this is not a necessary requirement in the numerical simulations. A derivation of these equations is given in Appendix A and details of the numerical simulations are given in Appendix B.

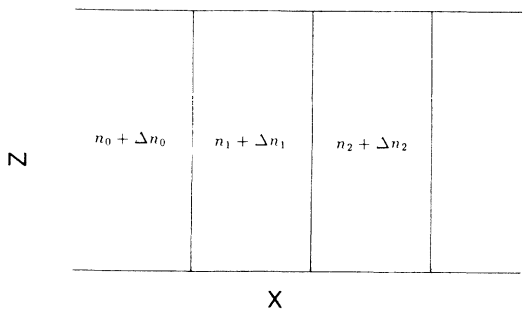

FIG. 1. Configuration of multilayered, self-focusing medium. x is the transverse and z the propagation direction.

We now specialize to a single interface which is located at $x=0$ such that $n=n_0$, and $\alpha=\alpha_0$ if $x<0$ and $n=n_1$, and $\alpha=\alpha_1$ if $x>0$. Let $2w_0$ be the beam waist in the medium and let $L_f=2\pi w_0^2/\lambda_0$, which is the Fresnel length. (λ_0 is the wavelength of the carrier in the vacuum.) Then the transformations $z/2\beta L_f\rightarrow z$, $ct/L_f\rightarrow t$, $x/w_0\rightarrow x$, and

$$F=\left[\frac{2}{\alpha_0}\right]^{1/2}\frac{\lambda_0}{2\pi w_0}\mathcal{E}\exp\left[i\left[\frac{2\pi w_0}{\lambda_0}\right]^2\left[\frac{n_0^2-\beta^2}{2\beta}\right]z\right]$$

reduce the basic equations above to the following perturbation form for each medium. For $x<0$

$$i\left[\frac{\partial\mathcal{E}}{\partial z}+\frac{2cn_0}{v_0}\frac{\partial\mathcal{E}}{\partial t}\right]=-\frac{\partial^2\mathcal{E}}{\partial x^2}-\delta\mathcal{E}\ ,$$
$$\tau_D\frac{\partial\delta}{\partial t}=-\delta+2|\mathcal{E}|^2\ , \tag{2}$$

and for $x>0$

$$i\left[\frac{\partial\mathcal{E}}{\partial z}+\frac{2cn_1}{v_1}\frac{\partial\mathcal{E}}{\partial t}\right]=-\frac{\partial^2\mathcal{E}}{\partial x^2}-(\delta-\Delta)\mathcal{E}\ ,$$
$$\tau_D\frac{\partial\delta}{\partial t}=-\delta+\frac{2}{\alpha}|\mathcal{E}|^2\ , \tag{3}$$

where $\Delta=2\pi L_f(n_0^2-n_1^2)/\lambda_0$ and $\alpha=\alpha_0/\alpha_1$, and v_i ($i=0,1$) are the group velocities in the left- and right-hand media, respectively. This choice of scaling is motivated by the fact that we will typically consider a cw beam, optical pulse, or pulse train, propagating initially in the left-hand medium ($x<0$). For an instantaneous nonlinear response ($\tau_D=0$) and a cw incident beam, Eq. (2) then becomes the dimensionless NLS equation for which the sech shape given below at $t=t_0$ is the $N=1$ soliton solution. As the self-trapped light channel, represented mathematically by this transverse spatial soliton, approaches the interface it will be deflected due to a finite but small perturbation due to the right-hand medium. We assume that $\alpha\approx 1$ and $\Delta\ll 1$, which makes the presence of the discontinuity at the interface a small perturbation on the underlying NLS equation. In steady state we recover the cw beam case studied in Ref. 1 where the underlying solutions are perturbed spatial solitons of the NLS equation. These coupled equations are solved by using a combination of the split-step method[10] and an algorithm due to Fleck[11] (see Appendix B). We choose as initial pulse profile a hyperbolic secant shape in x but modulated in time by a Gaussian or square profile. For example, the input Gaussian pulse shape is defined to be

$$2\eta\,\mathrm{sech}[2\eta(x-x_0)]\times\exp\left[i\frac{v(x-x_0)}{2}\right]\exp\left[-\left[\frac{t-t_0}{\tau_p}\right]^2\right]\ .$$

Here $v=4\pi\beta w_0\sin(\theta_0)/\lambda_0$, where θ_0 is the complement

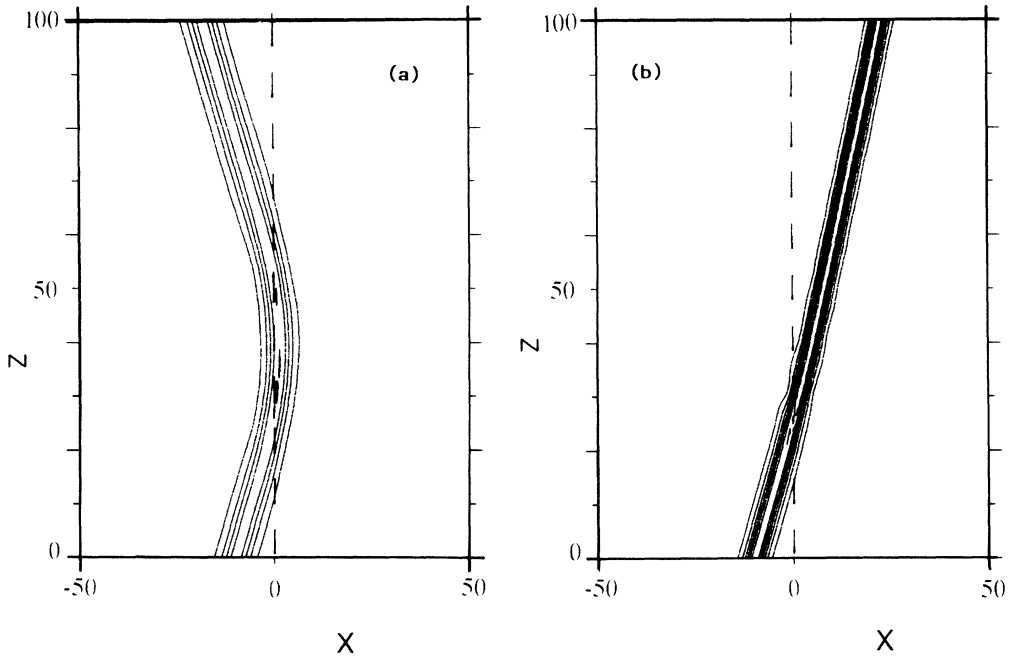

FIG. 2. cw beam reflection and transmission at the interface ($x=0$). (a) Low-power reflection with $2\eta=0.3938$. (b) High-power transmission with $2\eta=0.5906$. In both cases, $n_0=1.6$, $\Delta=0.1$, $\alpha_0=0.5$, $\alpha_1/\alpha_0=0.75$, and $v=0.4$.

to the angle of incidence of the optical pulse to the interface. The quantity v should not be confused with the group velocity v_i defined earlier. v represents a nondimensional soliton velocity and is related to the incident angle as defined above. The choice of sech shape is motivated by the fact that any incident localized profile in x will evolve to a sech profile for an instantaneously responding medium if it fulfills an appropriate area criterion as discussed in Ref. 12. Of course, the leading and trailing edges of the pulse will fail to satisfy this criterion and start to diffract. The nonlinear evolution problem defined by Eqs. (2) and (3) will take care of this distortion.

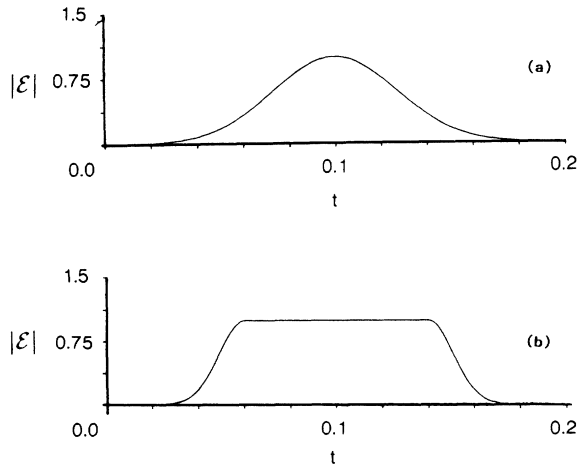

FIG. 3. Temporal profiles of initial conditions. (a) Gaussian; (b) square.

III. PULSE PROPAGATION IN INSTANTANEOUS RESPONDING NONLINEAR MEDIA

When the material responds instantaneously to the field ($\tau_D=0$), we can substitute $\delta=2|\mathcal{E}|^2$ in the left medium ($x<0$) and $\delta=(2/\alpha)|\mathcal{E}|^2$ in the right medium ($x>0$) equations above. Our first numerical check on the code reproduced the cw results reported in Ref. 1 for their parameter values: $\Delta=0.1$, $\alpha(=\alpha_1/\alpha_0)=0.75$, and $v=0.4$. The picture in Fig. 2(a) shows an incident self-trapped light channel reflecting from the nonlinear interface (dashed line) after suffering a significant lateral displacement from the geometric optics path. This is a manifestation of the nonlinear Goos-Hanchen shift.[1,2] A slight increment in power at the same fixed incidence angle leads to full transmission of the self-trapped beam. Both computations are carried out up to $z=100$ in our scaled units. Note that the self-trapped channel in the right medium is narrower due to the strong self-focusing effect in this medium. The total power in the channel is essentially the same as negligible radiation is generated at the interface and all of the energy remains in the transverse soliton.[1] The only change is a reshaping of the soliton in the left medium (shape determined by the parameters of that medium) into a soliton appropriate to the right medium. The success of the equivalent particle picture is based on the fact that this latter change is captured by the gradual change in the soliton's parameters as it reshapes while crossing the interface.[1]

The computation was now repeated for two types of incident optical pulse. The temporal profiles of the initial Gaussian and square pulses used are shown in Fig. 3. Figures 4(a) and 4(b) shows results of the time-dependent computation corresponding to the cw transmission case

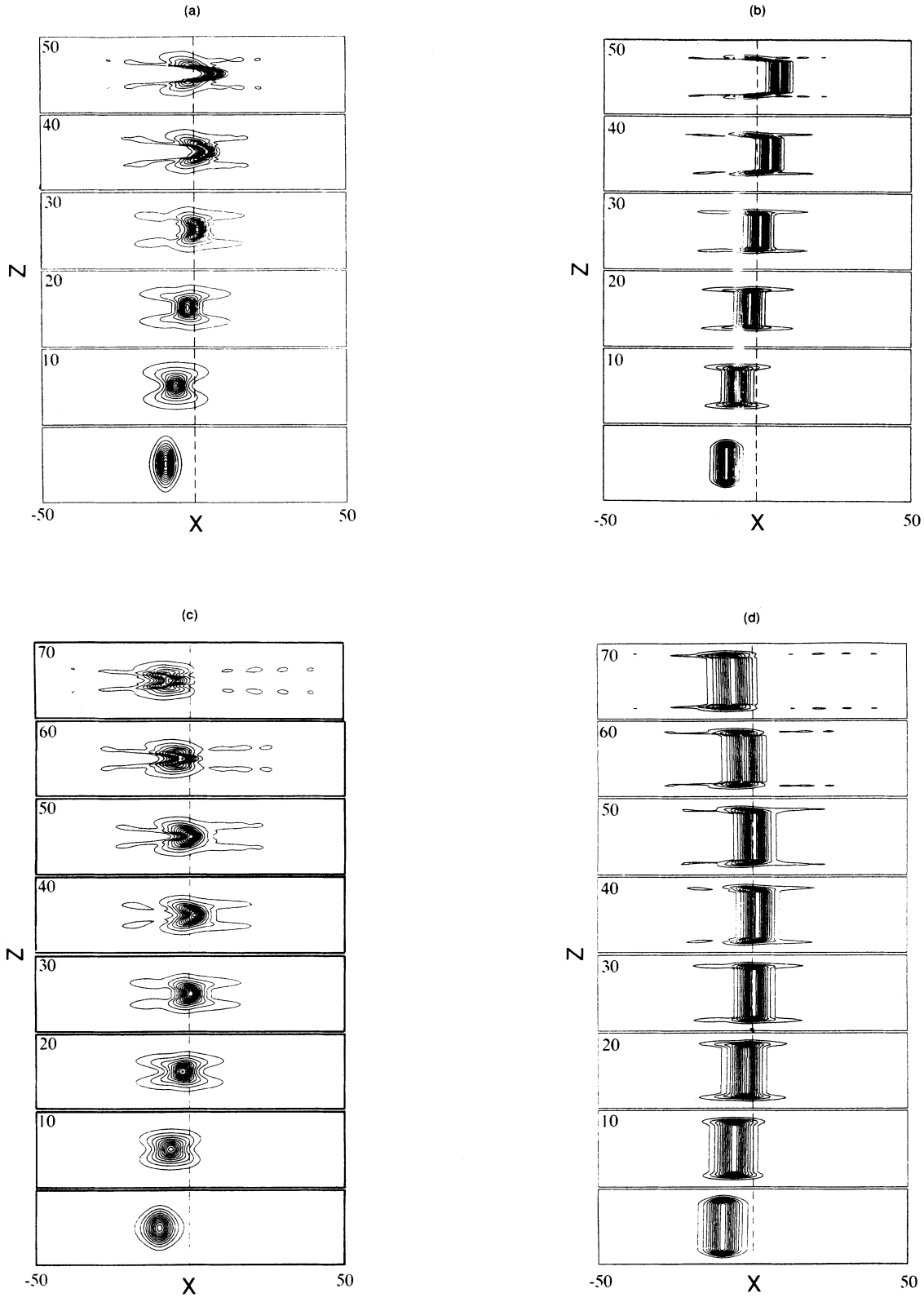

FIG. 4. Contour snapshots of pulses in media. (a) Transmission with the Gaussian pulse; (b) transmission with the square pulse; (c) reflection with the Gaussian pulse; (d) reflection with the square pulse. Each strip, i.e., a computational domain, extends by 0.4 units in the propagation direction z. The labels indicate the value of z of the top end of this strip as it moves in the medium starting at $z=0.4$. For example, $z=10$ means that the pulse profile is computed when it extends from $z=9.6$ to 10 within the medium. The parameter values are the same as in Fig. 2.

shown in Fig. 2(b). A contour plot of the pulse amplitude shows how the pulse distorts as it propagates in the medium up to $z=50$ in each case. The dashed line at the center indicates the location of the interface. The peak intensity of each pulse corresponds to the cw value used in generating Fig. 2(b). Since the center of each pulse corresponds to the transverse soliton shape used in Fig. 2(b), it follows the same trajectory as in Fig. 2(b). The pulse front and trailing ends diffract in the medium because these low-intensity parts feel a weaker self-focusing optical nonlinearity and they spread out eventually forming low-amplitude transverse solitons or linearly diffracting waves. The low-intensity part of each pulse is reflected and remains in the left medium as predicted by the equivalent particle theory. This is consistent with the cw computation in Fig. 2(a). This pulse stripping effect on transmission is more pronounced for the incident Gaussian pulse case depicted in Fig. 4(a) than for the incident square pulse in Fig. 4(b) due to its nonuniform amplitude variation. (Here the contour of the amplitude of a pulse is plotted as it propagates in the media.) This pulse stripping effect is due to the inability to maintain phase matching due to a nonuniform induced nonlinear phase change across the pulse profile. An identical problem arises in nonlinear optical switching using directional couplers. For completion, we include the pulsed version of reflection for both Gaussian and square optical pulses in Fig. 4(c) and 4(d), respectively. As expected the square pulse follows the cw beam reflected trajectory most closely. The most intense portion of the Gaussian pulse also follows the latter trajectory, although the leading and trailing edges suffer strong distortion.

The full integration of the Eqs. (3) and (4) was carried out up to $z=100$. The near-field time-integrated intensity of each pulse was computed at the exit of the nonlinear medium. Figure 5(a) shows the initial energy distribution of either pulse before it enters the medium. Figures 5(b) and 5(c) show the final energy distributions of the square

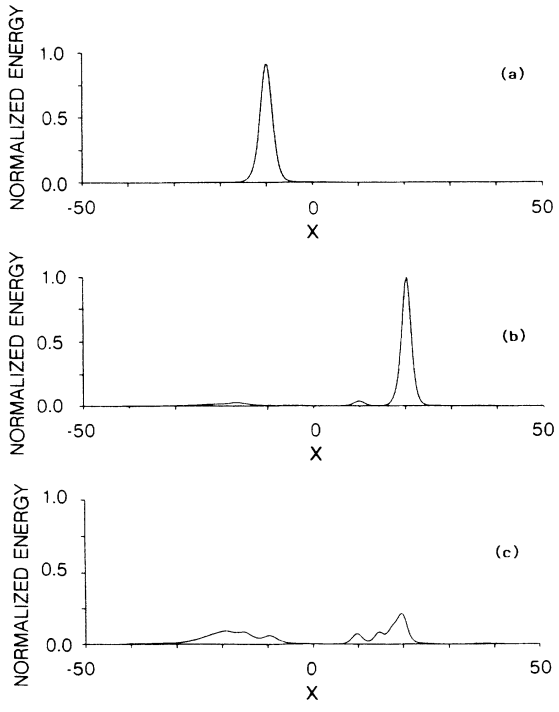

FIG. 5. Energy distributions of pulses. (a) Energy distribution of the initial condition; (b) energy distribution of the square pulse at $z=100$; (c) energy distribution of the Gaussian pulse at $z=100$.

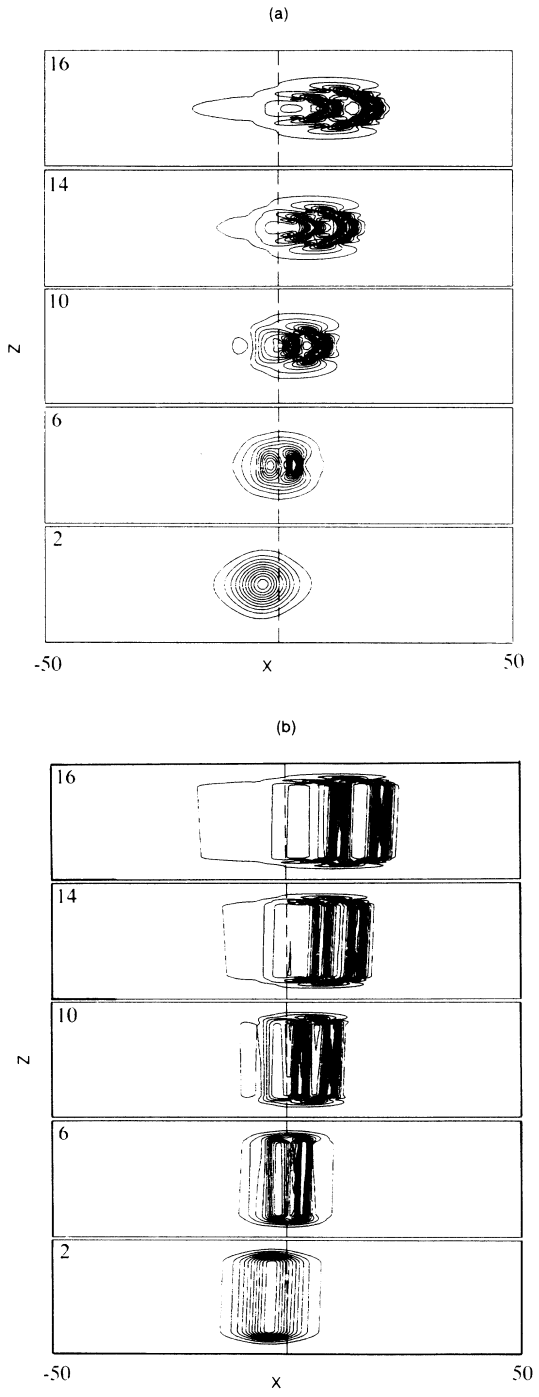

FIG. 6. Pulse breakup. (a) A Gaussian pulse breakup; (b) a square pulse breakup. In both cases, $\Delta=0.1$, $\alpha=0.125$, $\alpha_0=0.5$, $v=1.0$, and $2\eta=0.5$.

and the Gaussian pulse, respectively. If we take the full width at half-maximum (FWHM) of the initial energy distribution as a detector width located at the theoretical exit location as computed by the equivalent particle theory,[1] we find that with the square pulse, as much as 80% of the total energy is switched, whereas with the Gaussian only 23% is captured.

The phenomenon of light-channel breakup into multiple self-focused channels on transmission into the new medium was explained quantitatively by the theory in Ref. 1. This breakup phenomenon was explained in terms of the initial value problem for the NLS equation and accurate expressions were derived for the power in each individual channel and that channel's transmission angle. The question that we pose here is whether this breakup phenomenon will persist for transmitting Gaussian and square optical pulses. To ensure breakup into three light channels on transmission in the cw case, one needs to choose the nonlinear Kerr coefficient ratio appropriately. Choosing the same parameters as in Ref. 1 ($\alpha=0.125$, $\alpha_0=0.5$, $\Delta=0.1$, $v=1$), we repeated their calculation for both Gaussian and square pulses in an instantaneously responding Kerr medium. These results are shown as contour plots in Figs. 6(a) and 6(b). The pulse with the lowest amplitude is difficult to see in these plots. The center of each of the pulses follows exactly the same trajectory as the cw beam. Since the power of the Gaussian pulse varies continuously over its profile and therefore a different part of it excites a different amount of nonlinearity, its contour is generally contorted and no clear spatial breakup into separate channels is seen. On the other hand, with the exception at the pulse front and trailing end, the square pulse exhibits a much clearer breakup. If one connects each snapshot of square pulses in the medium contiguously, one obtains the cw trajectory.

IV. EQUIVALENT PARTICLE PICTURE

The above results can be interpreted using the equivalent particle theory[1] as follows. Since $\tau_D=0$, each temporal slice of the pulse evolves independently from the other. When the pulse is placed in the left medium as an initial condition, each slice evolves independently according to the nonlinear Schrödinger equation,

$$\frac{\partial \mathcal{E}}{\partial z}+\frac{2cn_0}{v_0}=i\frac{\partial^2 \mathcal{E}}{\partial x^2}+2i|\mathcal{E}|^2\mathcal{E} .$$

Let us write the pulse initial condition as

$$2\eta a(t)\,\mathrm{sech}(2\eta x)e^{ivx/2} , \tag{4}$$

where $0<t<0.2$ and $a(0.1)=1$ according to our choice as depicted in Fig. 3. We first want to know what transverse spatial soliton each temporal slice of (4) with a fixed t will evolve into if it stays in the left medium all of the time. Following Satsuma and Yajima,[13] we find that it evolves into a soliton of the form

$$2\bar{\eta}\,\mathrm{sech}(2\bar{\eta}x)e^{ivx/2} , \tag{5}$$

where $\bar{\eta}=\eta[2a(t)-1]$. The condition that each slice must satisfy in order that it evolve into an $N=1$ transverse spatial soliton is $0.5<a(t)<1.5$.

We now recall that in the equivalent particle theory, a soliton is specified by its coordinate $(\bar{x},v)$ in the phase space where $\bar{x}$ is the location of its center amplitude and v is its speed. The motion of the soliton in the medium, both left and right, is governed by

$$\frac{d^2\bar{x}}{dz^2}=-\frac{\partial U(\bar{x})}{\partial \bar{x}} . \tag{6}$$

The potential $U(\bar{x})$ is given by

$$U(\bar{x})=H(\bar{x})U_R(\bar{x},\eta_R)+[1-H(x)]U_L(\bar{x},\eta_L) , \tag{7}$$

where $H(\bar{x})$ is the Heaviside function, and U_R and U_L are potentials for the soliton in the left medium with its amplitude parameter η_L and that in the right medium with η_R, respectively. The two soliton parameters are related by $\eta_R=\eta_L\alpha_1/\alpha_0$.

We can construct an equivalent potential for each time slice of the initial pulse using (7), including the transla-

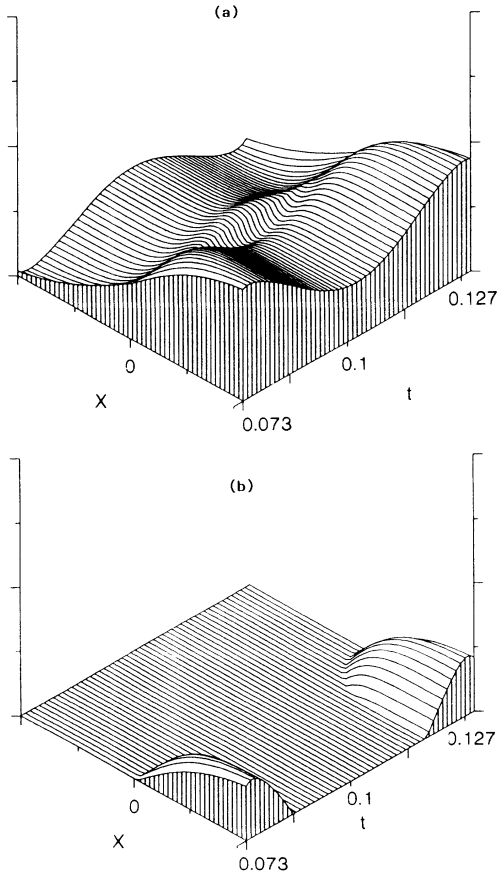

FIG. 7. Potential profiles for a Gaussian pulse. (a) The potential surface corresponding to the temporal slice of the Gaussian pulse in Fig. 3(a) for $0.073<t<0.127$. (b) The surface plot of potential energy minus total energy. Note that for $t<0.084$ and $t>0.116$. the potential energy is greater than the total energy. Therefore a transverse soliton which corresponds to any temporal slice in these two regions will be reflected at the interface.

tion factor $x-x_0$. Using the amplitude variation factor $a(t)$ corresponding to the Gaussian or the square pulse in Fig. 3 allows us to compute the equivalent potential at successive time intervals. Figure 7(a) shows the equivalent potential surface corresponding to an incident Gaussian pulse. This particular Gaussian amplitude profile has the form

$$a(t)=e^{-[(t-0.1)/0.038]^2} .$$

The potential shown is for $0.073<t<0.127$. Each temporal slice, which corresponds to a transverse soliton, has total energy given by $U[a(t),x_0]+v^2/2$ for each t. When we subtract the total energy from the potential surface, we obtain Fig. 7(b) where only the positive remainder is plotted. This tells us that at the pulse wings, the potential energy is larger than the total energy (represented by two humps symmetrically situated on each side of the beam center at $t=0.1$) and thus they are reflected at the interface. This reflected portion is found to be the pulse trailing edge in the range $0.116<t<0.2$ and the front edge in the range $0.0<t<0.084$ where $a(t)\leq 0.83$. In terms of energy, we find that 34.7% of the total energy of the initial pulse should be reflected and thus remain in the left medium and the rest is transmitted. The actual computation shows that the reflected energy for this case is 33.6%. The small discrepancy is due to the generated radiation not accounted for in the equivalent particle theory.

V. PULSE PROPAGATION IN NONLINEAR MEDIA WITH A FINITE TIME RESPONSE

If $\tau_D\neq 0$, the equivalent particle picture no longer strictly applies. Qualitatively, we can understand the effect of finite material response as follows. The front edge of the pulse will not experience the full impact of the nonlinear self-focusing, but instead will feel an accumulation of the nonlinear modification to the linear refractive index over a characteristic time τ_D. This integrating effect of the nonlinearity can be best appreciated by formally integrating the Debye equation (for example, for the left-hand medium)

$$\delta(x,z,t)=2\int_{-\infty}^{t}\frac{e^{-(t-t')/\tau_D}}{\tau_D}|\mathcal{E}(x,z,t')|^2dt' ,$$

where we assumed $\delta(x,z,-\infty)=0$. By integrating the right-hand side by parts, we see that $\delta(x,z,t)\approx 2(|\mathcal{E}|^2-\tau_D\partial|\mathcal{E}|^2/\partial t)$ for $\tau_D\ll 1$. Therefore we can approximate the beam propagation equation for short response time by

$$\frac{\partial\mathcal{E}}{\partial z}+\frac{1}{v_s}\frac{\partial\mathcal{E}}{\partial t}=i\frac{\partial^2\mathcal{E}}{\partial x^2}+2i\left[|\mathcal{E}|^2-\tau_D\frac{\partial|\mathcal{E}|^2}{\partial t}\right]\mathcal{E} .$$

This shows that a finite material response will reduce the effective nonlinearity at the leading edge of the pulse. As a specific example of the effect, we chose material parameters appropriate to CS_2 (Ref. 14) and considered transmission of a 30 ps (FWHM) Gaussian pulse with a spot size of 100 μm and $\lambda=1$ μm over a distance of 10 cm with $\tau_D=1$ ps. We assumed that the left medium is made of CS_2 and the right medium of some unknown material with its linear refractive index similar to that of CS_2 (the difference being less than 10^{-4}) and that the ratio of nonlinear coefficients α is 0.8. We also assume that the thickness of the film is 1 μm. Figure 8(a) shows contour plots of the pulse amplitude with its leading edge at 1, 2.5, 7.5 and 10 cm. The longitudinal (z-direction) spread of the pulse is about 1 cm. Thus the bottom picture shows the pulse just inside the medium and the second from bottom shows the pulse contour for 1.5 cm $<z<$ 2.5 cm and so forth. The complement to the angle of incidence for this case is 0.1° corresponding to $v=1$ and the peak pulse power of of 26 MW cm^{-2} was used. The strong diffraction of the leading edge of the pulse is evident from these pictures. In spite of the large amount of

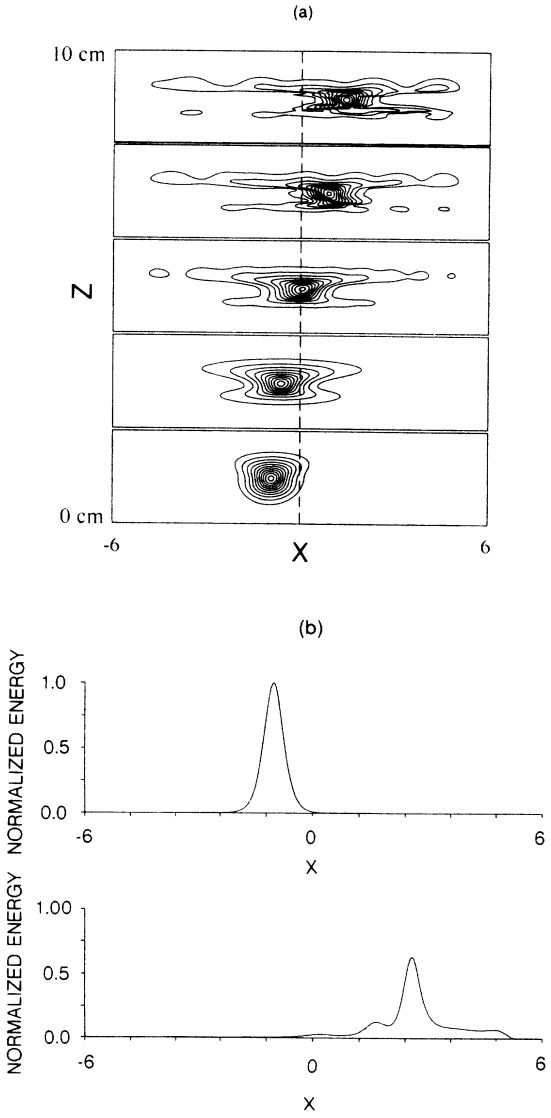

FIG. 8. Gaussian pulse propagation with nonzero τ_D. (a) From bottom to top the location of the pulse is 1, 2.5, 5, 7.5, and 10 cm. (b) Energy distribution as it exits the medium. The FWHM of the pulse is 30 ps and $\tau_D=1$ ps.

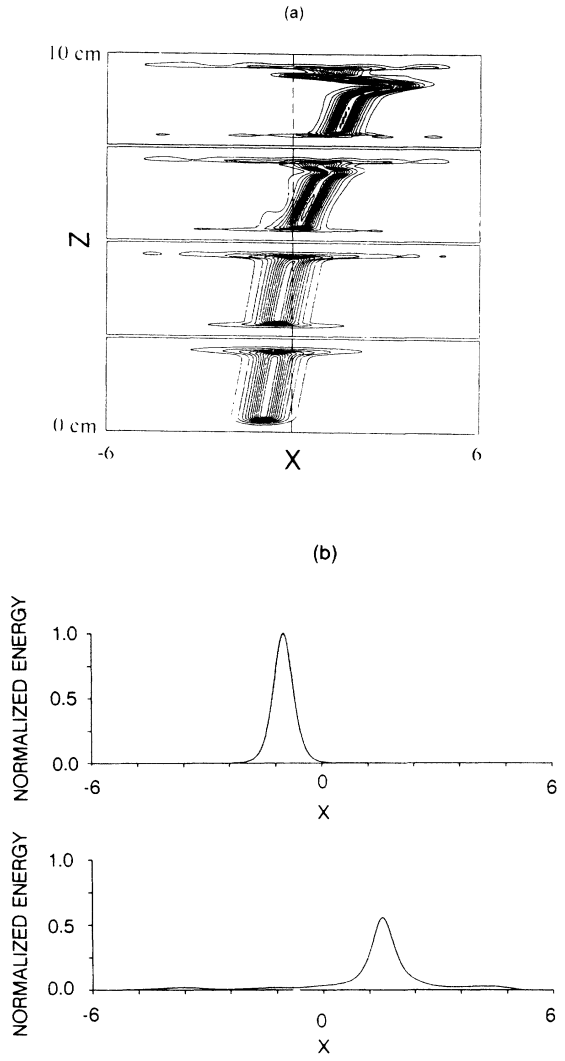

FIG. 9. Square pulse propagation with nonzero τ_D. (a) From bottom to top, the location of the pulse is 3, 5, 7.5, and 10 cm. (b) Energy distribution as it exits the medium. The FWHM of the pulse is 100 ps and $\tau_D=1$ ps.

diffraction, more than 44% of the total energy is localized around the maximum within the FWHM of the initial energy distribution as seen in Fig. 8(b). Figure 9(a) repeats the same computation but with a square pulse. Here the finite delay effect is very pronounced on the rapidly rising front of the pulse. The appearance of a radical twist in the top contour picture is conjectured to be due to the delay effect on the phase, therefore, the velocity of each transverse soliton. A full analysis of this phenomenon is currently under way. Comparing the two sets of pictures for the pulse energy distribution we see that the Gaussian pulse with finite time delay transmits at a shallower angle than the square pulse.

VI. DEMULTIPLEXING AND MULTIPLEXING OF OPTICAL PULSES

Our final computations provide a severe test of the equivalent particle picture. We consider a train of four square optical pulses propagating in an instantaneously responding Kerr medium. The pulses differ in peak amplitude by a few percent and in pulse energy by a fraction of a percent. We chose the worst possible case by working close to the critical angle where we expect that motion near the separatrix will be very sensitive to initial conditions. The idea is to see if the power adjustable cw spatial scanning operation in Ref. 12 can carry over to multiplexing incident optical pulses that are initially spatially separated into a single channel and demultiplexing an incident single channel into spatially separated pulses.

Figure 10(b) shows a train of four square pulses indexed by the numbers 1–4. Each square pulse has a transverse profile given by

$$2\eta a_i \mathrm{sech}[2\eta(x-\bar{x})]e^{i(v/2)x} .$$

In this particular case, we chose $2\eta=0.5906$, $a_1=0.92$, $a_2=0.95$, $a_3=1$, $a_4=1.08$, and $v=0.4$. From the above analysis, we know that the uniform intensity region of each square pulse evolves into transverse solitons whose new amplitude parameter is given by $\eta(2a_i-1)$. Once we know this, we can calculate the corresponding potential (7) and by integrating the equation (6) with this potential over the medium length, we can draw its trajectory. Figure 10(a) shows such trajectories of the individual pulses predicted by the equivalent particle theory. Their final positions at the end of the medium (at $z=100$) are $\bar{x}_1=-14.6$, $\bar{x}_2=3.5$, $\bar{x}_3=17.3$, and $\bar{x}_4=29.1$. Thus the pulse with the lowest intensity should be reflected according to the prediction. We next propagated this pulse train according to Eqs. (2) and (3). Figure 10(c) shows several contour pictures of the field in the medium. The energy profile at the end of the medium is plotted in Fig. 10(d) where the maxima occur at $\bar{x}_1=5.1$, $\bar{x}_2=13.2$, $\bar{x}_3=20.7$, and $\bar{x}_4=26.0$. The large discrepancy in the locations of the first and the second pulse is due to the combination of the following factors: (i) they are close to the critical trajectory which separates reflection from transmission, (ii) the equivalent particle theory assumes solitons whereas our initial conditions evolve to oscillatory solutions; and (iii) there is radiation as pulses cross the interface. This result shows that it is optimal to carry out such operations either entirely in transmission or reflection.

It is also possible to combine pulses (multiplexing) by taking advantage of power dependence of their trajectories. Suppose that we want all pulses coming out at the same location (x_f) and angle (v_f) from the medium after transmission. The initial location and angle of incidence of each pulse can be calculated by solving the equation of motion (6) backward in z. Figure 11(a) shows an example of such computation for $2\eta=0.5906$, $x_f=20$, and $v_f=0.4$ at $z=100$. The four square pulses shown in Fig. 11(b) have the amplitude coefficients $a_1=0.875$, $a_2=0.95$, $a_3=1.02$, and $a_4=1.1$. The four trajectories terminate in the left medium at the following positions in the phase space: $\bar{x}_1=-31.6$, and $v_1=0.628$, $\bar{x}_2=-28.3$, and $v_2=0.567$, $\bar{x}_3=-24.4$, and $v_3=0.492$, and $\bar{x}_4=-17.9$, and $v_4=0.37$. When we propagated the pulses according to our model, we get Fig. 11(c). Figure

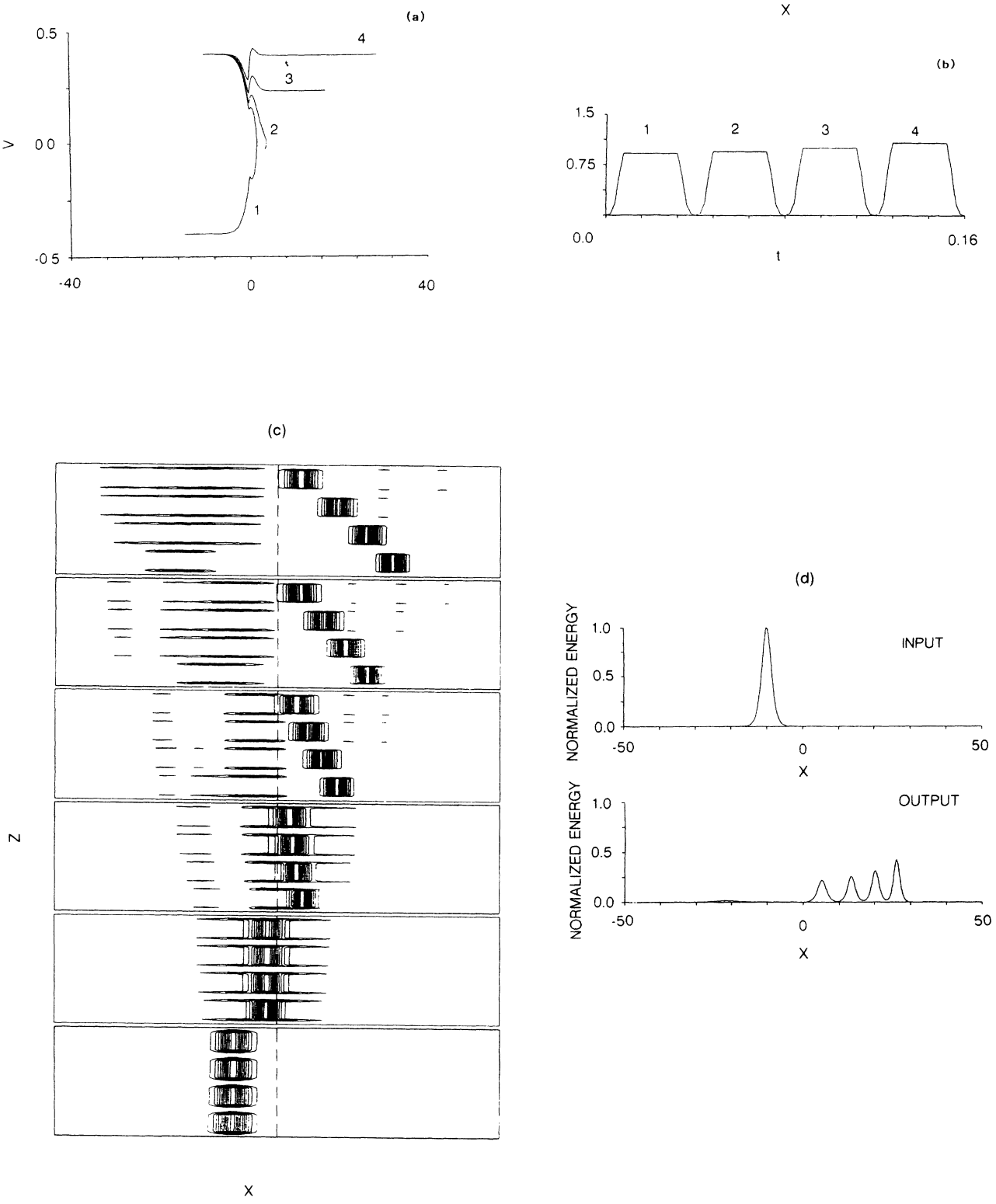

FIG. 10. Demultiplexing of square pulses. (a) Predicted trajectories of the pulses in the phase space. (b) Temporal profiles of the pulse train. From left to right, the amplitude factor is 0.92, 0.95, 1, and 1.08, respectively. (c) Contour plots of pulse amplitude at $z=1$, 10, 40, 70, and 100, respectively. (d) Energy distributions. Top at $z=0$, bottom at $z=100$. With $\alpha_0=1.5$, $\alpha=0.75$, $\Delta=0.1$, and $v=0.4$.

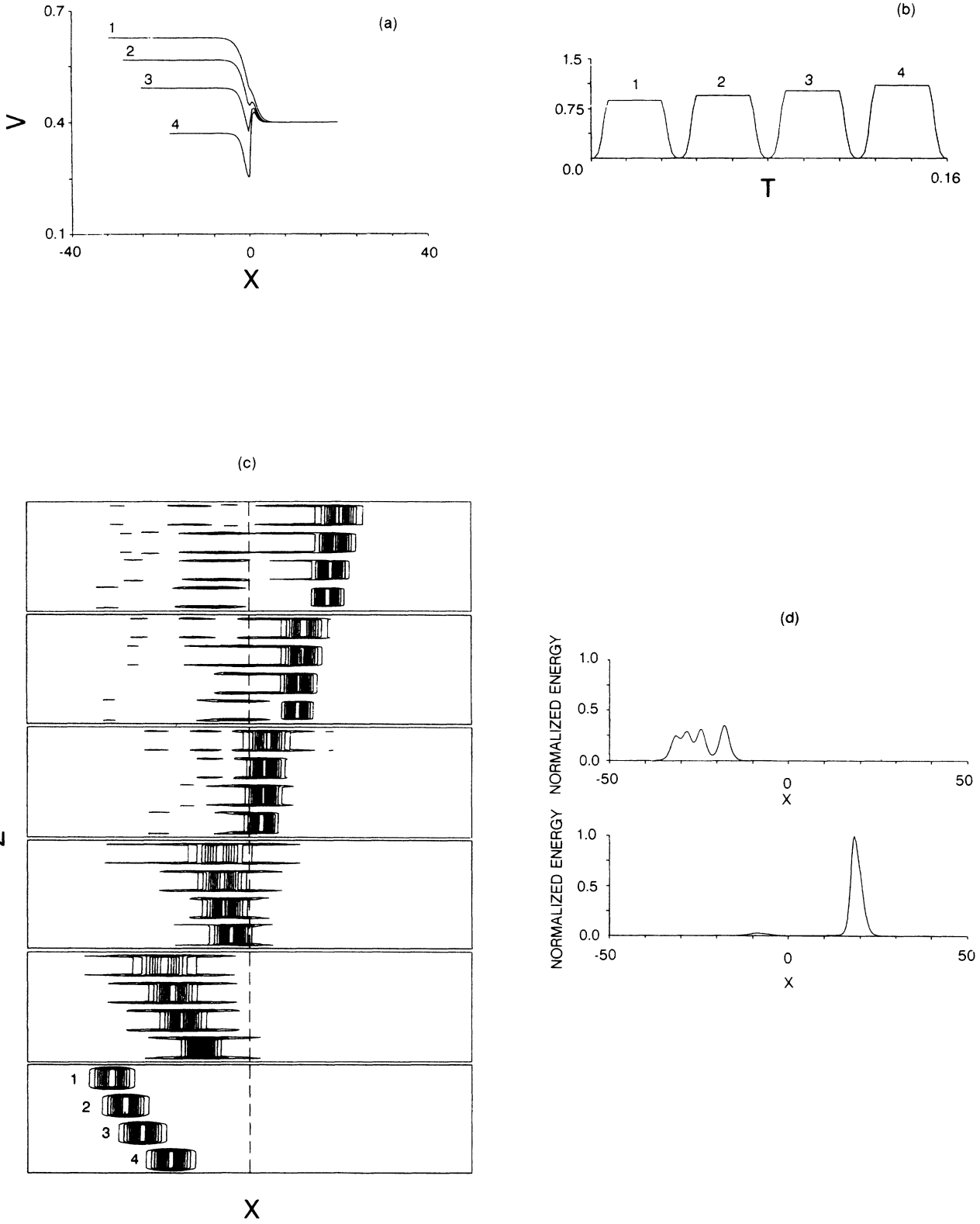

FIG. 11. Multiplexing of square pulses. (a) Predicted trajectories in the phase space. (b) Temporal profiles of the pulse train. From left to right, the amplitude factor is 0.875, 0.95, 1.02, and 1.1, respectively. (c) Contour plots of the pulse amplitude. The locations are the same as in Fig. 10(c). (d) Energy distributions. Top at $z=0$; bottom at $z=100$. The material parameters are the same as in Fig. 10.

11(d) shows the field energy profile at the end of the medium. The full numerical results agree quite well with the simple predictions.

VII. CONCLUSIONS

We have shown in this paper that power-controlled nonlinear optical switching of short optical pulses can be achieved rather easily at a single interface separating two nonlinear self-focusing media. The effect of finite material response will place a limit on the minimum optical pulse length if the switching is to remain clean and predictable. The equivalent-particle theory in Ref. 1 remains a powerful predictive tool in anticipating the overall behavior of the pulse reflection and transmission characteristics. Not surprisingly, square pulses yield the highest contrast switching due to their fast rise times and flat intensity profiles. Group velocity dispersion has not been included in the model as we feel that its effect will be small over the short lengths needed for pulse switching. Our computations confirm that many of the predictions of the cw beam theory in Ref. 1 remain valid under pulsed conditions.

ACKNOWLEDGMENTS

This work was supported by the Boeing Company High Technology Center, Seattle. Partial support was provided under a United Kingdom Science and Engineering Research Council (SERC) Grant No. GR/D84726.

APPENDIX A

To derive our basic equations we assume that the field obeys the wave equation

$$\nabla^2\mathbf{E}-\frac{1}{c^2}\frac{\partial^2\mathbf{D}_L}{\partial t^2}=\frac{1}{c^2}\frac{\partial^2(\delta\mathbf{E})}{\partial t^2} \tag{A1}$$

and the Debye equation

$$\tau_D\frac{\partial\delta}{\partial t}=-\delta+\alpha|\mathbf{E}|^2 ,$$

where τ_D is the Debye relaxation time. We assume that the electric field is quasimonochromatic and linearly polarized and one transverse dimensional (in x only), that is,

$$\mathbf{E}=\mathbf{e}F(x,z,t)e^{i(\beta k_0 z-\omega_0 t)} ,$$

where k_0 is the wave number in vacuum at ω_0. The linear electric displacement is written as

$$\mathbf{D}_L=\left[\int_{-\infty}^{\infty}\epsilon(\omega_0+\Delta\omega)\hat{\mathbf{E}}(\omega_0+\Delta\omega)e^{i\Delta\omega t}d(\Delta\omega)\right]\times e^{i(\beta k_0 z-\omega_0 t)} ,$$

which is substituted in (8). Keeping only the first-order term in the right-hand side of (8), the propagation equation then becomes

$$\frac{\partial^2 F}{\partial z^2}+2ik_0\beta\left[\frac{\partial F}{\partial z}+\frac{nk_0'}{\beta}\frac{\partial F}{\partial t}\right]+\frac{\partial^2 F}{\partial x^2}-k_0^2[\beta^2-(n^2+\delta)]F-(k_0'^2+nk_0k_0'')\frac{\partial^2 F}{\partial t^2}+\cdots=0 , \tag{A2}$$

where the ellipsis represents higher-order terms. Here n is the linear refractive index of the medium, $k_0'(=\partial k/\partial\omega|_{\omega=\omega_0})$ and $k_0''(=\partial^2 k/\partial\omega^2|_{\omega=\omega_0})$ are the group velocity and the group velocity dispersion of the field in the medium at ω_0, respectively. In particular, $k(\omega_0)=nk_0$. Under the slowly varying envelop approximation, we drop the second z and t derivatives from (9). We then obtain our basic equations (1).

APPENDIX B

To numerically solve Eqs. (2) and (3), we use the split-step method whose efficiency and speed are well proven especially with a nonlinear Schrödinger equation.[10] As the name suggests, the split-step method *splits* the right-hand side of each of the propagation equations into two parts, i.e., the linear part, which consists of the dispersion term $(\partial^2\mathcal{E}/\partial x^2)$ and the nonlinear part, which consists of all the rest. We advance a given initial condition separately using these two and combine the results in a way consistent with the full *unsplit* equation. The linear part is solved by the fast Fourier transform and the nonlinear part by Fleck's scheme[11] as will be discussed below. There are two key ideas involved in our strategy. One is how to deal with a slight difference in the propagation speed of a field across the interface. The other is how to minimize storage requirements in computation.

The field propagates at the characteristic speed of $v_0/2cn_0$ in the left medium and at $v_1/2cn_1$ in the right medium. This poses some problem to us since the split-step method uses the Fourier transformation in its linear part, scanning the solution at some z in the whole transverse domain across the interface. If the solution on the left side of the medium lags behind that on the right (because usually $n_0>n_1$), we could not apply the split-step method. To get around this, we solve the nonlinear parts for different time steps in the left and right medium so that we have the whole solution at the same longitudinal location z, ready to be Fourier transformed. This artificial time asynchronization is usually insignificant since $n_0\approx n_1$.

It seems natural to discretize the medium and propagate the pulse through it, computing and updating the field profile every Δz. However, this requires use of an array of large dimensions especially when the propagation distance is large. Since there is no dispersion in the time or the longitudinal direction, a pulse localized in these directions stays localized. We take advantage of this fact and write a code which, in essence, propagates the medium through the pulse. An initial pulse is defined in the vacuum and stored in a stack, say, $\mathcal{E}(1),\ldots,\mathcal{E}(n)$. [See Fig. 12(a).] Here, for example, $\mathcal{E}(1)$ contains a com-

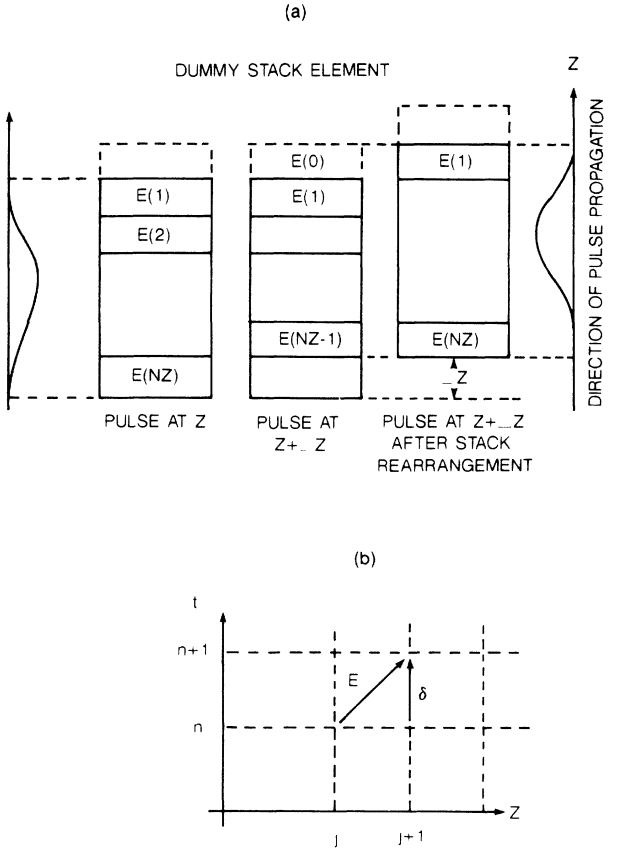

FIG. 12. (a) Stack management. The amount of storage space remains constant and independent of the propagation distance. (b) Fleck's scheme. The field information propagates along its characteristic but the nonlinearity propagates upward along the time direction.

plete transverse profile of the pulse front and $\mathcal{E}(n)$ a complete transverse profile of the pulse trailing edge. (There is also a corresponding δ stack.) As the whole pulse propagate over Δz in the medium, the field stack looks like $\mathcal{E}(0),\ldots,\mathcal{E}(n-1)$. We rearrange the stack indices such that this new solution is stored back in $\mathcal{E}(1),\ldots,\mathcal{E}(n)$. This process is repeated. The total dimension of storage arrays remains $(nz+1)nx$, where nz is the number of longitudinal nodes of the pulse and nx that of its transverse nodes. This enables us to propagate a pulse for a long distance without any additional memory space.

The nonlinear part of the equations is solved by Fleck's method[10] together with Newton iteration. Look, for example, at the nonlinear part in the left medium. It is of the form

$$\frac{\partial\mathcal{E}}{\partial z}+\frac{2cn_0}{v_0}\frac{\partial\mathcal{E}}{\partial t}=i\delta\mathcal{E}\ , \tag{B1}$$

which is coupled with

$$\frac{\partial\delta}{\partial t}=-\frac{1}{\tau_D}\delta+\frac{2}{\tau_D}|\mathcal{E}|^2\ . \tag{B2}$$

Given Δz (the longitudinal step), we let $\Delta t=(2cn_0/v_0)\Delta z$. [$\Delta t=(2cn_1/v_1)\Delta z$ in the right medium.] Then, following Fleck, we write

$$\mathcal{E}_{j+1}^{n+1}-\mathcal{E}_j^n=i\frac{\Delta z}{2}(\delta_{j+1}^{n+1}\mathcal{E}_{j+1}^{n+1}+\delta_j^n\mathcal{E}_j^n)\ ,$$

together with

$$\delta_{j+1}^{n+1}=C\delta_{j+1}^n+A|\mathcal{E}_{j+1}^n|^2+B|\mathcal{E}_{j+1}^{n+1}|^2\ ,$$

where

$$A=2\left[\frac{\tau_D}{\Delta t}(1-e^{-\Delta t/\tau_D})-e^{-\Delta t/\tau_D}\right]\ ,$$

$$B=2\left[1-\frac{\tau_D}{\Delta t}(1-e^{-\Delta t/\tau_D})\right]\ ,$$

$$C=e^{-\Delta t/\tau_D}\ ,$$

and n and j are the time node index and the longitudinal node index, respectively. [See Fig. 12(b)]. The linear analysis shows that this is a third-order scheme. This system of difference equations are solved for $\mathcal{E}_{j+1}^{n+1}$ and δ_{j+1}^{n+1} by a simple Newton iteration scheme. The iteration scheme involves the inversion of a 2×2 matrix at each step. A typical computation involves arrays of the size 256×100 and depending on the propagation distance, it takes 10 min to nearly an hour on Cray X-MP. Accuracy of computation is checked by monitoring the total pulse energy, a conserved quantity in our model. Additionally, convergence of the solution was confirmed by using smaller step sizes.

[1]A. B. Aceves, J. V. Moloney, and A. C. Newell, Phys. Rev. A **39**, 1809 (1989); **39**, 1828 (1989); Phys. Lett. **129A**, 231 (1988).
[2]W. J. Tomlinson, J. P. Gordon, P. W. Smith, and A. E. Kaplan, Appl. Opt. **21**, 2041 (1982).
[3]R. Cuykendall, and K. Strobl, J. Opt. Soc. Am. B **6**, 877 (1989).
[4]M. Miyagi, and S. Nishida, Sci. Rep. Res. Inst. Tohuku Univ. Ser. B **25**, 53 (1973); W. J. Tomlinson, Opt. Lett. **5**, 323 (1980); see A. A. Maradudin, in *Optical and Acoustic Waves in Solids-Modern Topics,* edited by M. Borissov (World Scientific, Singapore, 1983), p. 72.
[5]D. R. Andersen, Phys. Rev. A **37**, 189 (1988).
[6]P. Varatharajah, A. B. Aceves, J. V. Moloney, D. R. Heately, and E. M. Wright, Opt. Lett. **13**, 609 (1988).
[7]P. Varatharajah, A. B. Aceves, and J. V. Moloney, J. Opt. Soc. Am. B **7**, 220 (1990).
[8]A. M. Weiner,, J. P. Heritage, R. J. Hawkins, R. N. Thurston, E. M. Kirschner, and W. J. Tomlinson, Phys. Rev. Lett. **61**, 2445 (1988).
[9]J. V. Moloney, Phys. Rev. A **36**, 4563 (1987).
[10]T. R. Taha, and M. J. Ablowitz, J. Comput. Phys. **55**, 203 (1984).
[11]A. J. Fleck, Phys. Rev. B **1**, 84 (1970).
[12]P. Varathrajah, A. B. Aceves, and J. V. Moloney, Appl. Phys. Lett. **54**, 2631 (1989).
[13]J. Satsuma, and N. Yajima, Prog. Theor. Phys. Suppl. **55**, 284 (1974).
[14]S. Manueif, R. Desailly, and C. Froehly, Opt. Commun. **65**, 193 (1988).